Talanta 120 (2014) 304–311

Contents lists available at ScienceDirect

Talanta

journal homepage: www.elsevier.com/locate/talanta

Well-dispersed Pt nanoparticles on polydopamine-coated ordered mesoporous carbons and their electrocatalytic application

Lijiao Yan, Xiangjie Bo, Dongxia Zhu, Liping Guo*

Faculty of Chemistry, Northeast Normal University, Changchun 130024, PR China

ARTICLE INFO

Article history:
Received 15 October 2013
Received in revised form
10 December 2013
Accepted 14 December 2013
Available online 19 December 2013

Keywords:
Ordered mesoporous carbons
Polydopamine
Pt nanoparticles
Hydrogen peroxide
Hydrazine

ABSTRACT

Polydopamine (PDA)-coated ordered mesoporous carbons (OMCs) are easily prepared through one-step self-polymerization of dopamine on OMCs matrix at room temperature. Pt nanoparticles (NPs) are deposited on OMCs-PDA *via* a simple chemical reduction. The PDA layer helps to improve the water-solubility and dispersibility of OMCs, and plays a key role in the deposition of uniform and well-distributed Pt NPs. Transmission electron microscopy images reveal that the ultra-fine Pt NPs with an average size of ~1.8 nm are well-dispersed on the surface of OMCs-PDA. The electrocatalytic behavior of OMCs-PDA/Pt modified glassy carbon (GC) electrode is investigated by cyclic voltammetry and current–time methods using hydrogen peroxide (H_2O_2) and hydrazine (N_2H_4) as redox probes. Results show that OMCs-PDA/Pt exhibits improved electrocatalytic activity towards H_2O_2 reduction and N_2H_4 oxidation compared with OMCs/Pt. The linear electro-redox responses are found for H_2O_2 and N_2H_4 in the range of 2–14324 μM and 1–229 μM with the detection limit (S/N=3) of 0.85 μM and 0.51 μM, respectively. In addition, this new nanocomposite modified electrode exhibits high sensitivity, good anti-interference ability, excellent reproducibility and long-term stability.

1. Introduction

Highly ordered mesoporous carbons (OMCs) have been receiving much attention since their discovery by Ryoo et al. in 1999 [1]. The introduction of metal nanoparticles (NPs) further extends the application of OMCs and provides new good features such as catalytic and electrochemical properties [2–4]. Uniform distribution and small particle size of metal NPs can expand their surface area and thus maximize the electrochemical and catalysis activity of metal NPs [5]. Studies have reported that surface functionalization can introduce more binding sites and surface anchoring groups on OMCs, which facilitated the absorption of metal precursor on OMCs and the obtainment of well-dispersed metal NPs with small particle size. For example, sulfur-modified OMCs [6], concentrated nitric acid (HNO_3)-treated OMCs [7], and polypyrrole (PPy)-coated OMCs [8] were used as supports for Pt NPs. Results showed that the average particle size of Pt NPs supported on modified OMCs was smaller than that supported on original OMCs. However, OMCs treated with concentrated HNO_3 for 2 h could partially destroy the initial ordered structure of OMCs [9]. The process of PPy polymerization needed an extra radical initiator [8]. As a consequence, a simple and versatile modification method is still urgent to simultaneously control the particle size and the distribution of Pt NPs.

Recently, Messersmith et al. proposed polydopamine (PDA), a kind of biopolymer, which could be formed on a wide range of inorganic and organic materials through self-polymerization of dopamine (DA) in alkaline solution at room temperature [10]. The *in situ* spontaneous polymerization of DA provides the advantages of one-step surface functionalization with simple ingredients, mild reaction condition, and applicability to various types of materials. PDA layer can improve the surface properties, such as wettability and biocompatibility of multiwalled carbon nanotubes (MWCNTs) [11], stability and dispersibility of graphene oxide (GO) [12]. Moreover, PDA as a melanin-like material is an amorphous organic semiconductor and has abundant amine and hydroxyl groups, which are helpful for the grafting of charged metal complex that can be transformed into metal NPs upon reduction [11] and are beneficial for the anchoring and dispersion of metal NPs [13,14]. In comparison with MWCNTs and GO, OMCs are a promising matrix for Pt nanomaterials owing to their periodic structure, large surface area and high pore volume [15,16]. Their accessible ordered pores can provide sufficient room for mass transport. Hence, it is reasonable to functionalize OMCs with PDA in order to improve the water-solubility and dispersibility of OMCs, which is beneficial for OMCs to effectively absorb Pt precursor. More importantly, with the help of PDA, well-dispersed and small Pt NPs with high electrocatalytic activity are likely to be obtained.

* Corresponding author. Tel./fax: +86 04 3185 099 762.
E-mail address: guolp078@nenu.edu.cn (L. Guo).

0039-9140/$ - see front matter © 2013 Elsevier B.V. All rights reserved.
http://dx.doi.org/10.1016/j.talanta.2013.12.031

Hydrogen peroxide (H_2O_2), is not only a by-product of a large number of oxidase enzymes, but also an essential intermediate in biomedical, food production, pharmaceutical, industrial and environmental fields [17]. Hydrazine (N_2H_4) is widely used in areas such as pharmaceutical intermediates, fuel cells, manufacture of antioxidants, rocket propellants, pesticides, blowing agents, explosives, and textile dyes [18]. Therefore, the rapid and accurate detection of H_2O_2 and N_2H_4 is of great significance. There are many techniques including fluorescence, titrimetric, spectrophotometry, chemiluminescence and electrochemistry methods for the detection of H_2O_2 [19–22] and N_2H_4 [23–26]. Among these analytical techniques, electrochemical detection is distinctive for its high sensitivity, selectivity and simplicity.

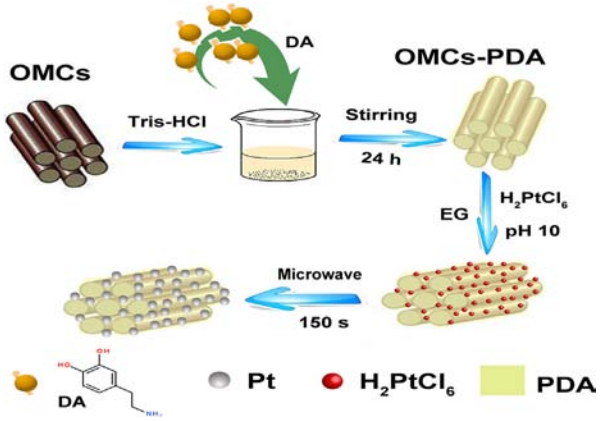

Scheme 1. Illustration of the preparation of OMCs-PDA/Pt nanocomposite.

In this work, PDA-coated OMCs are easily prepared through one-step self-polymerization of DA on OMCs matrix at room temperature without any hard acid or radical initiator treatment. The presence of PDA on the OMCs facilitates the obtainment of ultra-fine Pt NPs with good dispersion and small particle size. Compared with OMCs/Pt and OMCs, the OMCs-PDA/Pt modified electrode exhibits improved electrocatalytic activity towards H_2O_2 reduction and N_2H_4 oxidation, which proves that the as-synthesized OMCs-PDA/Pt can be used as electrochemical sensors and biosensors.

2. Experimental

2.1. Reagents and apparatus

Pluronic P123 (non-ionic triblock copolymer, $PEO_{20}PPO_{70}$-PEO_{20}) and Nafion (5 wt %) were purchased from Sigma-Aldrich, while $H_2PtCl_6 \cdot 6H_2O$ and 2-amino-2-hydroxymethylpropane-1,3-diol (Tris, $C_4H_{11}NO_3$) were purchased from Sinopharm Chemical Reagent Co. Ltd. The 0.1 M phosphate buffer solution (PBS pH 7.0), which was made up from NaH_2PO_4, Na_2HPO_4 and H_3PO_4, was employed as a supporting electrolyte. All other chemicals were at least of analytical grade. Aqueous solutions were prepared with doubly distilled water and stored in the shade.

Electrochemical experiments were performed on a CHI 660C electrochemical workstation (CH Instruments, China) connected to a personal computer. A three-electrode configuration was employed, consisting of a modified glassy carbon (GC) electrode (3 mm diameter) serving as a working electrode, whereas an Ag/AgCl (in saturated KCl solution) and a platinum wire served as the reference and counter electrodes, respectively. Infrared (IR) spectrum of the

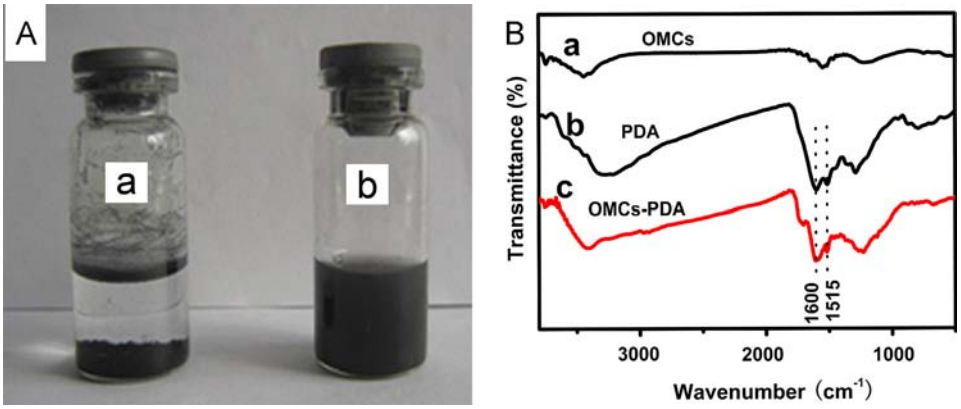

Fig. 1. (A) Photographs of vials containing 2.0 mg mL^{-1} of (a) OMCs and (b) OMCs-PDA in aqueous solution for three weeks after sonication treatment. (B) IR spectra of (a) OMCs, (b) PDA and (c) OMCs-PDA.

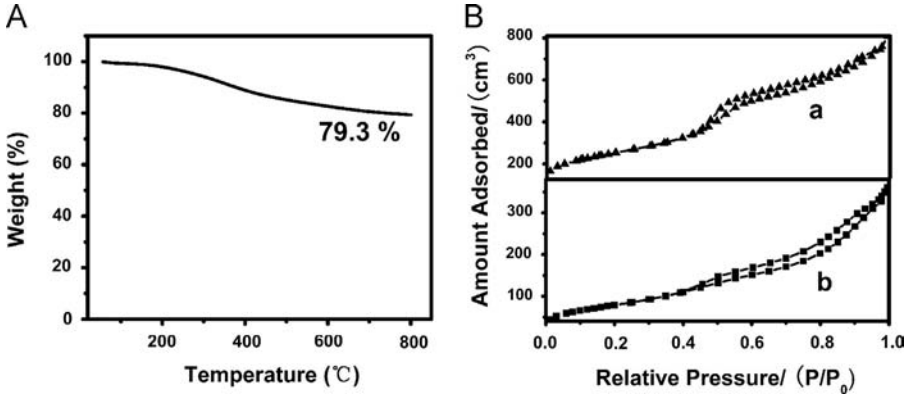

Fig. 2. (A) TGA curve of OMCs-PDA in N_2 atmosphere. (B) Nitrogen adsorption–desorption isotherms for (a) OMCs and (b) OMCs-PDA nanocomposite.

sample was recorded with Nicolet Magna 560 FT-IR spectrometer with a KBr plate. Nitrogen adsorption–desorption isotherms were performed on ASAP 2020 (Micromeritics, USA). The specific surface area was calculated by the Brunauer–Emmett–Teller (BET) method. The pore size was obtained from the desorption branch of the isotherm by the Barrett–Joyner–Halenda method. The total pore volume was determined from the amount of liquid nitrogen adsorbed at a relative pressure of about 0.99. Thermogravimetric analysis (TGA) was performed on a PerkinElmer Diamond TG Analyzer. X-ray diffraction (XRD) patterns were obtained on an X-ray D/max-2200vpc (Rigaku Corporation, Japan) instrument operated at 40 kV and 20 mA and using Cu Kα radiation (k=0.15406 nm). Transmission electron microscopy (TEM) images were obtained using a JEM-2100 F transmission electron microscope (JEOL, Japan) operating at 200 kV. X-ray Photoelectron Spectroscopy (XPS) was measured using Thermo ESCA LAB spectrometer (USA).

Table 1
Textural parameters of OMCs and OMCs-PDA nanocomposite.

Samples	Pore diameter (nm)	BET surface area ($m^2\ g^{-1}$)	Pore volume ($cm^3\ g^{-1}$)
OMCs	4.0	900	1.28
OMCs-PDA	3.1	290	0.54

2.2. Synthesis of OMCs, OMCs-PDA, OMCs/Pt and OMCs-PDA/Pt nanocomposites

The silica template SBA-15 was synthesized using Pluronic P123 as the surfactant and tetraethyl orthosilicate as the silica source [27]. OMCs were prepared according to the method reported by Ryoo et al. [28]. OMCs-PDA nanocomposite was obtained by the following procedure: 60 mg of OMCs was dissolved in 40 mL of Tris–HCl (pH 8.5, 10 mM) buffer solution. The mixture was first ultrasonically treated for 15 min to ensure that OMCs were uniformly dispersed in Tris–HCl buffer solution. Next, 30 mg of DA was added, and the solution was stirred at room temperature for 24 h. The PDA-coated OMCs were then separated by centrifugation and washed with deionized water several times, dried in a vacuum oven at 70 °C for 24 h and designated as OMCs-PDA. Pt NPs were deposited on OMCs-PDA by a chemical reduction of $H_2PtCl_6 \cdot 6H_2O$. In a typical procedure, 50 mg of OMCs-PDA were dispersed in 60 mL of ethylene glycol (EG) containing 234 μL of $H_2PtCl_6 \cdot 6H_2O$ (0.1 g mL^{-1}). The pH value was adjusted to 10.0 by dropping 0.5 M KOH in EG to induce small and uniform Pt NPs formation [29]. After being immediately sonicated for

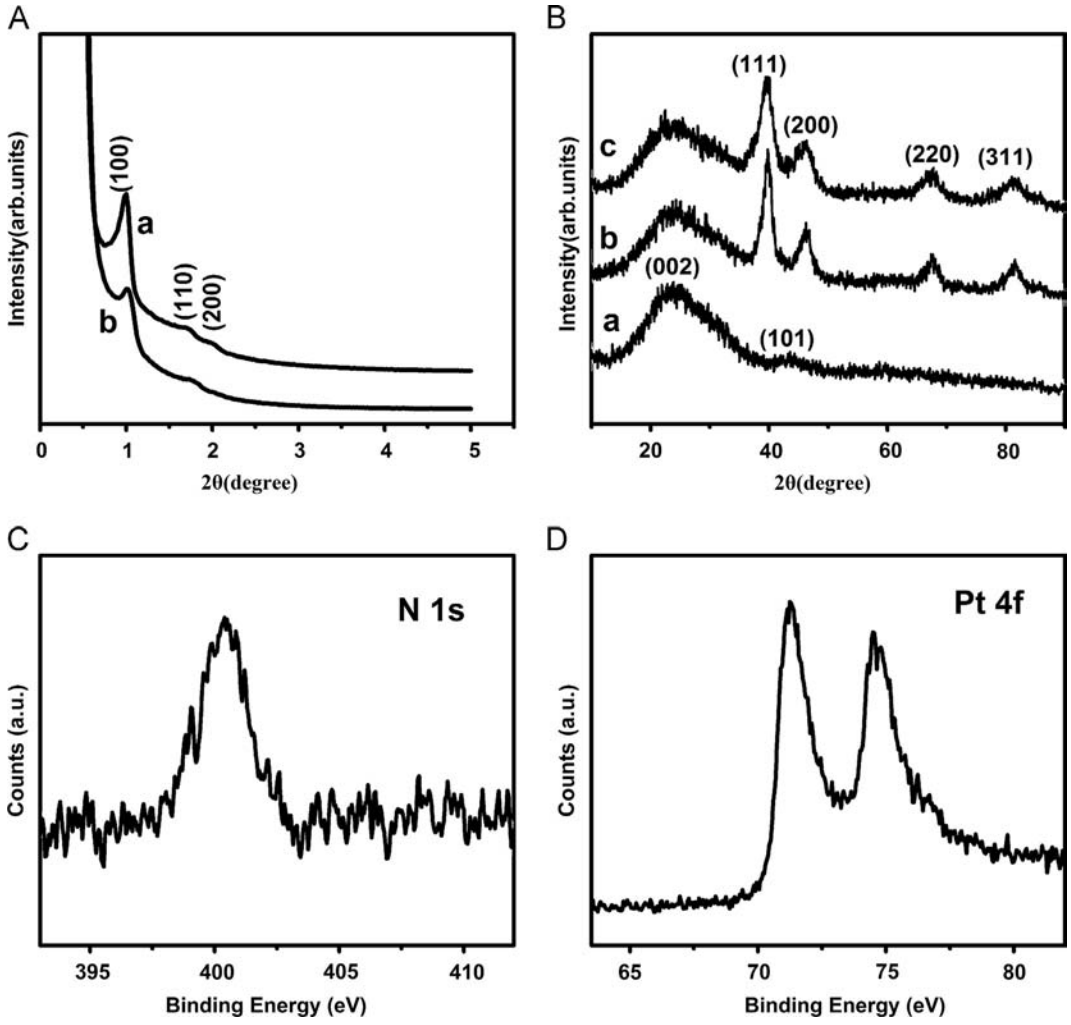

Fig. 3. (A) Small-angle XRD of (a) OMCs and (b) OMCs-PDA nanocomposite. (B) Wide-angle XRD of (a) OMCs, (b) OMCs/Pt and (c) OMCs-PDA/Pt nanocomposites. XPS of (C) N1s and (D) Pt4f of OMCs-PDA/Pt nanocomposite.

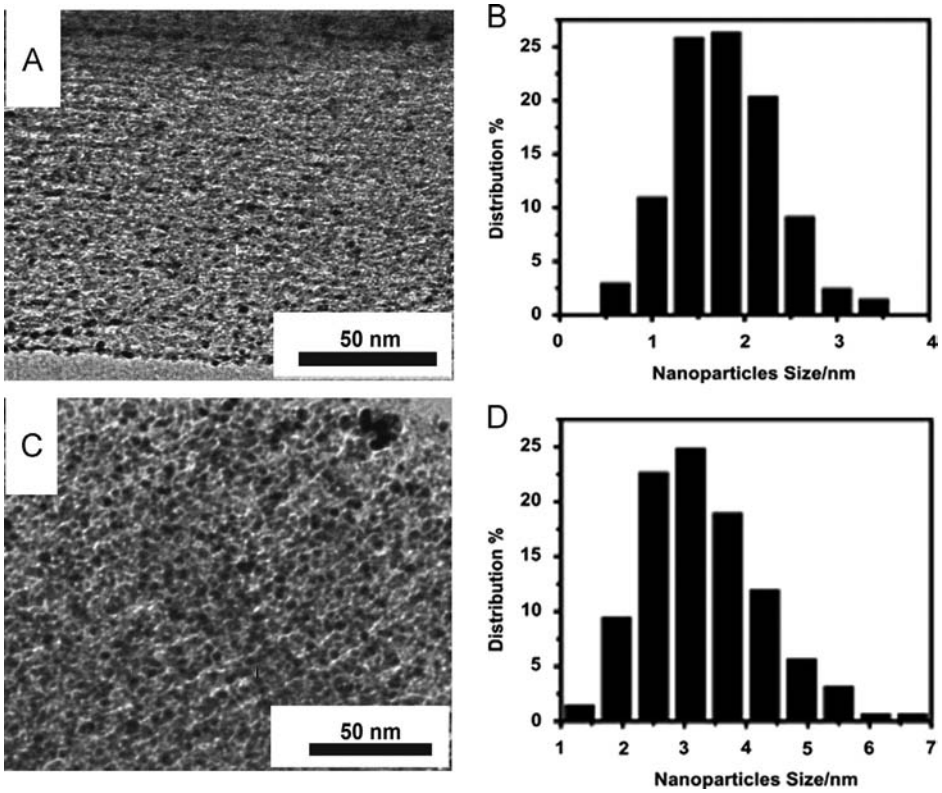

Fig. 4. TEM image and columnar distribution of Pt NPs size for OMCs-PDA/Pt (A and B) and OMCs/Pt nanocomposites (C and D).

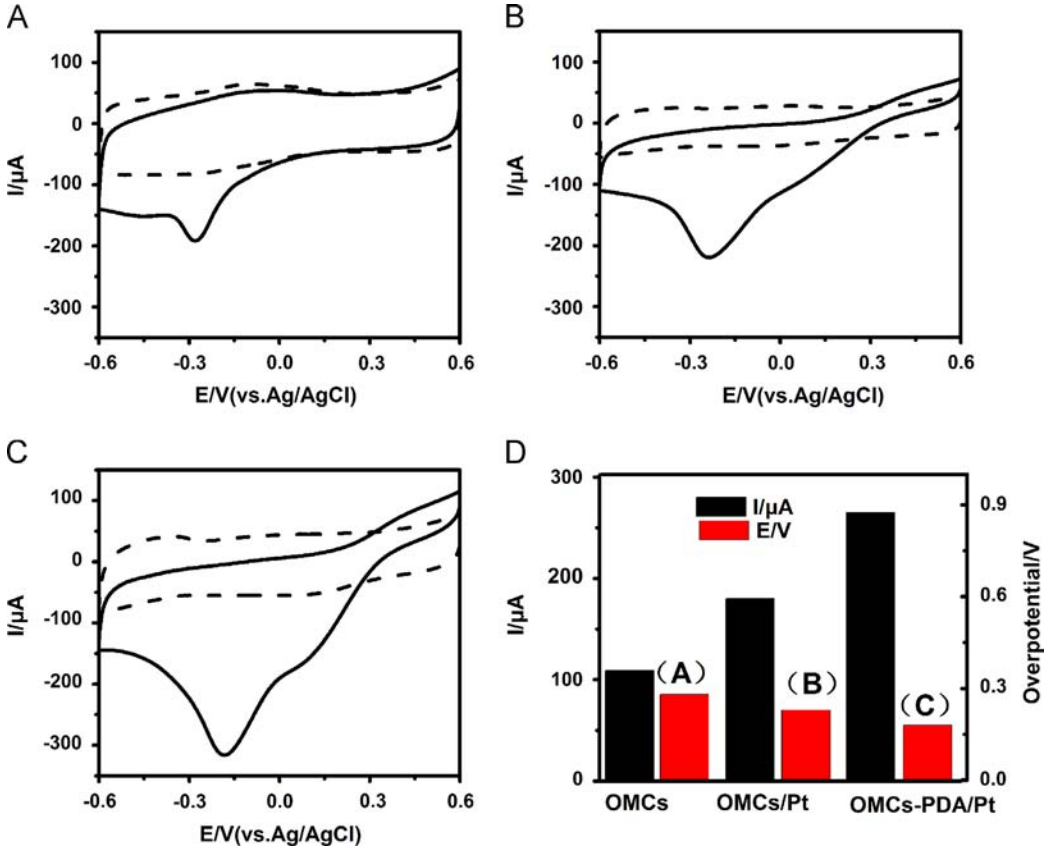

Fig. 5. CVs of (A) OMCs/Nafion/GC, (B) OMCs/Pt/Nafion/GC and (C) OMCs-PDA/Pt/Nafion/GC (c) electrodes in 0.1 M PBS (pH 7.0) containing 0 mM (dash line) and 5 mM (solid line) H_2O_2 at 50 mV s^{-1}. (D) The corresponding over-potential and background-corrected current relationship of different modified electrodes.

about 10 min, the solution was placed in the microwave oven for 150 s (power: 800 W Galanz). The fast heating by microwave accelerates the reduction of the metal precursor and the nucleation of the metal clusters [30]. The reaction mechanism is shown in the following equations [31]:

$$HOCH_2CH_2OH \rightarrow CH_3CHO + H_2O$$

$$2CH_3CHO + [PtCl_6]^{2-} + 6OH^- \rightarrow 2CH_3COO^- + Pt + 6Cl^- + 4H_2O$$

Then, the solution was centrifuged and washed several times with deionized water and dried in a vacuum oven at 70 °C for 48 h. The obtained products were designated as OMCs-PDA/Pt. The preparation of OMCs-PDA/Pt nanocomposite is illustrated in Scheme 1. As a comparison, OMCs/Pt nanocomposite was also prepared using the same procedure except for the PDA modification.

2.3. Preparation of the modified electrode

GC electrode (3 mm diameter) was polished before each experiment with 1, 0.3 and 0.05 μm alumina power, rinsed thoroughly with doubly distilled water between each polishing step, and dried in air. Approximately 1 h of ultrasonication was necessary to disperse 2 mg OMCs, OMCs/Pt or OMCs-PDA/Pt into a mixture of 0.1 mL (5 wt %) Nafion and 0.9 mL distilled water. After dropping 5 μL of the suspension onto the bare electrode surface, the electrode was dried in air at laboratory temperature.

3. Results and discussion

3.1. Characterization of OMCs, OMCs-PDA, OMCs/Pt and OMCs-PDA/Pt

Fig. 1A shows the photographs of OMCs (a) and OMCs-PDA (b) in aqueous solution for three weeks after sonication treatment. As can be seen in Fig. 1A, after three weeks, OMCs (a) appear as heterogeneous aggregates, and can be clearly found at the bottom of the vial. However, a uniform and well-distributed solution of OMCs-PDA (b) is observed in the aqueous solution to the naked eye, indicating that OMCs are successfully wrapped by PDA, in which abundant amino and catechol groups of PDA contribute to their good dispersibility and water-solubility. Fig. 1B exhibits IR spectra of (a) OMCs, (b) PDA and (c) OMCs-PDA. As can be seen in Fig. 1B (c), after OMCs coated by PDA, several new absorption bands appear. The typical absorption peak at 1600 cm^{-1} is attributed to the superposition of N–H bending and phenylic C=C stretching vibrations, and the peak at 1515 cm^{-1} is related to aromatic C–H bending vibration of PDA [32,33]. The result proves the formation of PDA layer on the OMCs surface.

The attachment of the PDA to OMCs was evidenced by TGA. As shown in Fig. 2A, the release of the PDA occurs at 352 K, which is mainly due to the thermal decomposition of PDA in N_2 atmosphere. The weight ratio of the PDA to OMCs is estimated to be 0.21:0.79. Fig. 2B presents the nitrogen adsorption–desorption isotherms of OMCs (a) and OMCs-PDA (b). The resulting sorption isotherms are both type IV isotherms with a pronounced capillary condensation step, characteristic of high-quality mesoporous materials. It is observed that the isotherm changes considerably after OMCs coated by PDA. First, the adsorption capacity decreases after the incorporation of PDA. Second, the shift of the capillary condensation step to lower relative pressure evidences a decrease of the pore size. The textural parameters of the OMCs and OMCs-PDA are summarized in Table 1. The PDA partially occupies the pores of OMCs and nitrogen molecules cannot access the surface of pores, so the BET surface area of OMCs-PDA decreases compared with OMCs matrix. The total pore volumes of OMCs-PDA are smaller than that of OMCs, which also suggest that PDA has been successfully coated on OMCs matrix.

The influence of incorporation of PDA on the mesostructure of OMCs was also investigated by XRD. Fig. 3A displays the typical small-angle XRD patterns of OMCs (a) and OMCs-PDA (b). The synthesized OMCs are replicas of the parent templates SBA-15 [27]. After the incorporation of PDA, the existence of the main diffraction peak (100) illustrates that the framework hexagonal ordering of OMCs is basically retained. The marked intensity decrease of OMCs-PDA diffraction peaks is related to the growth of PDA in the framework of OMCs. Fig. 3B displays the wide-angle XRD patterns of OMCs (a), OMCs/Pt (b) and OMCs-PDA/Pt (c). The ordered arrangements of the carbon materials give rise to the well-resolved XRD peaks. Two broad diffraction peaks at 2θ of 23.8° and 43.7° are observed at OMCs sample (a), corresponding to the (002) and (101) diffractions of graphite. Several peaks appeared in the wide-angle XRD patterns of OMCs/Pt and OMCs-PDA/Pt (b and c). The four peaks between 30° and 90° correspond to the (111), (200), (220) and (311) Pt facets. These patterns are in good agreement with the reference pattern (JCPDS 65-2868) for Pt [34,35], demonstrating that Pt NPs exist in OMCs/Pt and OMCs-PDA/Pt nanocomposites. In addition, the Pt NPs for the two samples have the same face-centered cubic crystal structure.

The formation of OMCs-PDA/Pt was characterized by XPS. Fig. 3C and D exhibits XPS patterns of N1s and Pt4f for OMCs-PDA/Pt nanocomposite, respectively. The N1s XPS spectrum clearly

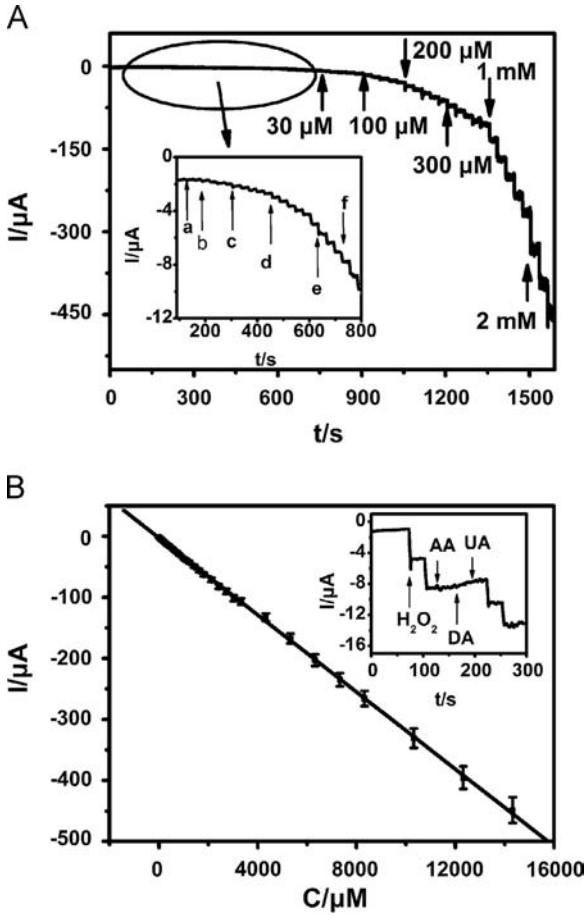

Fig. 6. (A) The amperometric *i–t* curve of OMCs-PDA/Pt with successive additions of H_2O_2 at the potential of −0.18 V. Inset shows the amplification of amperometric response of (a) 1, (b) 2, (c) 3, (d) 10, (e) 20, and (f) 30 μM H_2O_2. (B) The corresponding calibration plot for H_2O_2 (RSD=4.7%, n=5). Inset shows the amperometric response of OMCs-PDA/Pt towards 0.1 mM H_2O_2, AA, DA, and UA at −0.18 V, respectively.

demonstrates the existence of N element in OMCs-PDA/Pt material. The presence of N1s peak is due to the amino groups of PDA. In Pt4f XPS spectrum, the Pt 4f7/2 and 4f5/2 lines appear at 71.3 and 74.7 eV, respectively. These demonstrate the formation of Pt (0) state [36], which further supports the conclusion that OMCs-PDA/Pt nanocomposite has been successfully synthesized.

TEM was used to characterize the morphology and dispersion of Pt NPs. Fig. 4A shows that well-dispersed Pt NPs are facilely supported on the framework of the OMCs-PDA. Fig. 4B illustrates the corresponding histogram of the particle size distribution of Pt. On counting more than 400 particles, the average diameter is found to be 1.8 nm, as shown in the histogram. And no obvious Pt NPs aggregation is clearly observed on the surface of OMCs-PDA. However, Pt NPs supported on OMCs without modification of PDA are poorly dispersed and partially aggregated to large regiments (Fig. 4C). Their particle sizes are between 1 and 7 nm (Fig. 4D) with a mean size of 3.3 nm, which is much larger than those of Pt NPs supported on OMCs-PDA. These results reveal that OMCs-PDA nanocomposite provides an obvious advantage for achieving high-quality OMCs-PDA/Pt nanocomposite with Pt NPs of good dispersion and small particle size. This is due to PDA layer which can improve the dispersibility and water-solubility of OMCs and thus introduce more binding sites and surface anchoring groups on OMCs to effectively absorb metal precursor. The abundant amino and catechol groups of PDA are helpful for uniformly grafting charged metal complex that can be transformed into metal crystals upon reduction, leading to smaller crystal size of the Pt NPs [11].

3.2. Direct electrocatalysis and amperometric detection of H_2O_2

Fig. 5A presents the cyclic voltammograms (CVs) of OMCs/Nafion/GC (A), OMCs/Pt/Nafion/GC (B) and OMCs-PDA/Pt/Nafion/GC

Table 2
Comparison of the performance of various H_2O_2 sensors.

Electrode	Linear range (mM)	Detection limit (μM)	Sensitivity (μA mM^{-1} cm^{-2})	Potential applied (V)	Reference
Pt/PPy[a]/GC	1–8	1.2	80.4	−0.1 (vs.Ag/AgCl)	[22]
Pd/PEDOT[b]/GC	0.0025–1	2.84	215.3	−0.2 (vs.Ag/AgCl)	[37]
Pt/PEDOT[b]/SPC[c]	0.5–3.9	1.6	19.29	−0.55 (vs.Ag/AgCl)	[38]
Cu_2O/GNs[d]/GC	0.3–7.8	20.8	–	−0.4 (vs.Ag/AgCl)	[39]
DNA-AgCNs[e]/GNs[d]/GC	0.015–2.3	3.0	–	−0.7 (vs. SCE)	[40]
PDA-Ag	0.092–20	–	–	−0.30 (vs. SCE)	[41]
OMCs-PDA/Pt/GC	0.002–14.32	0.85	447	−0.18 (vs.Ag/AgCl)	This work

[a] Polypyrrole.
[b] Poly(3,4-ethylenedioxythiophene).
[c] Screen-printed carbon.
[d] Graphene.
[e] Polynucleotide-templated silver nanoclusters.

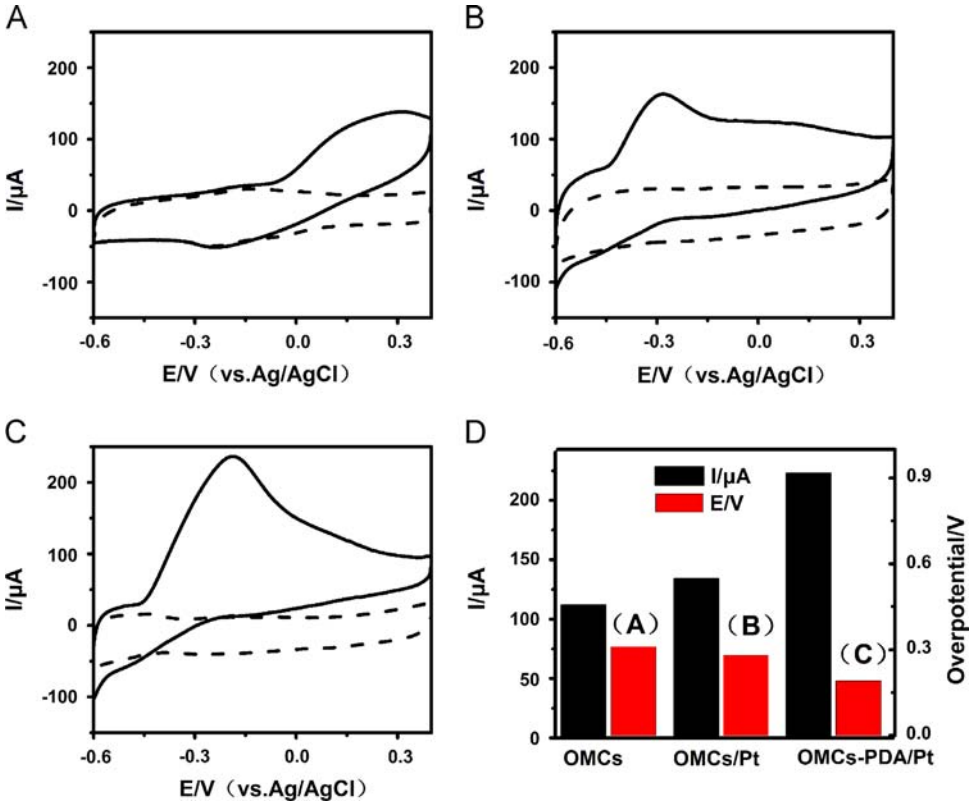

Fig. 7. (A) CVs of (A) OMCs/Nafion/GC, (B) OMCs/Pt/Nafion/GC and (C) OMCs-PDA/Pt/Nafion/GC (c) electrodes in 0.1 M PBS (pH 7.0) containing 0 mM (dash line) and 5 mM (solid line) N_2H_4 at 50 mV s^{-1}. (D) The corresponding over-potential and background-corrected current relationship of different modified electrodes.

(C) electrodes in 0.1 M PBS (pH 7.0) containing 0 mM (dash line) and 5 mM (solid line) H_2O_2 at 50 mV s^{-1}. As can be seen, the maximum peak value of reduction current on OMCs-PDA/Pt/Nafion/GC (C) electrode is −314 μA, higher than those of OMCs/Nafion/GC (A) and OMCs/Pt/Nafion/GC (B). The peak potential for the reduction of H_2O_2 on OMCs-PDA/Pt/Nafion/GC electrode is −0.18 V, which is more positive than that on OMCs/Nafion/GC and OMCs/Pt/Nafion/GC electrodes, shifting positively by about 100 mV and 50 mV, respectively. In order to investigate the electrocatalytic activities of different modified electrodes more clearly, Fig. 5D shows the corresponding over-potential and background-corrected current relationship of three modified electrodes. The higher background-corrected current and lower over-potential suggest that the OMCs-PDA/Pt catalyst exhibits much better electrocatalytic activity towards the reduction of H_2O_2 than OMCs/Pt and OMCs. Due to the excellent electrochemical properties of the OMCs-PDA/Pt/Nafion/GC electrode, we used this material for research in the following work.

Fig. 6A shows the typical amperometric *i*–*t* curve of OMCs-PDA/Pt/Nafion/GC with successive additions of H_2O_2 at the potential of −0.18 V. The OMCs-PDA/Pt/Nafion/GC electrode has linear chronoamperometric responses to H_2O_2 concentrations between 2 and 14324 μM with the linear regression equation of I (A)=0.0316C (M)+2.6×10^{-6} (R=0.999, n=47). The sensitivity is calculated as 447 μA mM^{-1} cm^{-2} (the slope of calibration plot divided by geometric surface area of GC electrode). The detection limit is 0.85 μM with the signal-to-noise ratio of three (S/N=3). A comparison of linear range, sensitivity, detection limit and applied potential for OMCs-PDA/Pt modified electrode with other H_2O_2 sensors reported in literature is shown in Table 2. The data reveal that the analytical parameters for OMCs-PDA/Pt modified electrode are comparable and even better than those obtained at several electrodes reported recently. The interference effect of dopamine (DA), uric acid (UA), and ascorbic acid (AA) on the determination of H_2O_2 is studied (inset of Fig. 6B). As can be seen, the OMCs-PDA/Pt/Nafion/GC electrode produces negligible amperometric signal for 0.1 mM DA, UA and AA. The low operating potential is responsible for good ability of anti-interference to the co-existing electroactive molecules. The reproducibility of the sensor was also investigated. The relative standard deviation of the amperometric response towards 5 mM H_2O_2 is less than 4.2% for five repetitive measurements at the same electrode. When the OMCs-PDA/Pt/Nafion/GC electrode was stored at 4 °C for two weeks, the amperometric response for 5 mM H_2O_2 remained 93.6% of its original value, suggesting the long-term stability of the electrode.

3.3. Direct electrocatalysis and amperometric detection of N_2H_4

Fig. 7A displays the CVs for the oxidation of 0 mM (dash line) and 5 mM (solid line) N_2H_4 on OMCs/Nafion/GC (A), OMCs/Pt/Nafion/GC (B) and OMCs-PDA/Pt/Nafion/GC (C) electrodes in 0.1 M PBS (pH 7.0) at 50 mV s^{-1}. The anodic current is about 237 μA at the OMCs-PDA/Pt/Nafion/GC (C) electrode, compared to 164 μA at the OMCs/Pt/Nafion/GC (B) and 137 μA at the OMCs/Nafion/GC (A) electrode. Moreover, the obvious oxidation peak of N_2H_4 is observed at −0.19 V on OMCs–PDA/Pt/Nafion/GC electrode, the peak potential is lower than that of the OMCs/Pt/Nafion/GC (−0.28 V) electrode. We also exhibited the corresponding over-potential and background-corrected current relationship of the three modified electrodes in Fig. 7D. It is obvious that OMCs-PDA/Pt/Nafion/GC reflects the superior performance over OMCs/Pt/Nafion/GC and OMCs/Nafion/GC towards the oxidation of N_2H_4. The improved electrocatalytic performance of OMCs-PDA/Pt towards H_2O_2 reduction and N_2H_4 oxidation is ascribed to the following possible reasons. First, the modification of PDA improves the dispersibility and water-solubility of OMCs and thus helps to introduce more binding sites and surface anchoring groups on OMCs to effectively absorb metal precursor. Second, the abundant amino and catechol groups of PDA play a key role in the conjunction with $[PtCl_6]^{2-}$ and are beneficial for the anchoring and dispersion of these Pt NPs. The ultra-fine Pt NPs on OMCs-PDA with an average size of ~1.8 nm could supply more surface-active sites for the adsorption of reactants. As a result, enhanced electrocatalytic activities towards H_2O_2 reduction and N_2H_4 oxidation are obtained from OMCs-PDA/Pt.

Fig. 8A shows the typical amperometric *i*–*t* curve at OMCs-PDA/Pt/Nafion/GC electrode with successive additions of N_2H_4 at −0.19 V. A linear detection range from 1 to 229 μM is obtained at OMCs-PDA/Pt/Nafion/GC electrode. The regression equation is I (A)=0.1869C (M)−3.1×10^{-6} (R=0.998, n=35). The OMCs-PDA/Pt/Nafion/GC biosensor exhibits a high sensitivity of 2645 μA mM^{-1} cm^{-2} (the slope of calibration plot divided by geometric surface area of GC electrode), which is higher than those of ZnO-Fluorine doped tin oxide glass electrode (44.24 μA mM^{-1} cm^{-2}) [26], polyaniline-graphene composited thin film electrode (325.4 μA mM^{-1} cm^{-2}) [42] and Pd–TiO_2 electrode (554 μA mM^{-1} cm^{-2}) [43]. The detection limit is 0.51 μM with the signal-to-noise ratio of three (S/N=3). We also investigated the interference effect of some common compounds in the environmental system on the determination of N_2H_4 (inset of Fig. 8B). It is clear that the Mg^{2+}, NH_4^+, K^+, SO_4^{2-}, Cl^- and NO_3^- have no obvious influence on the

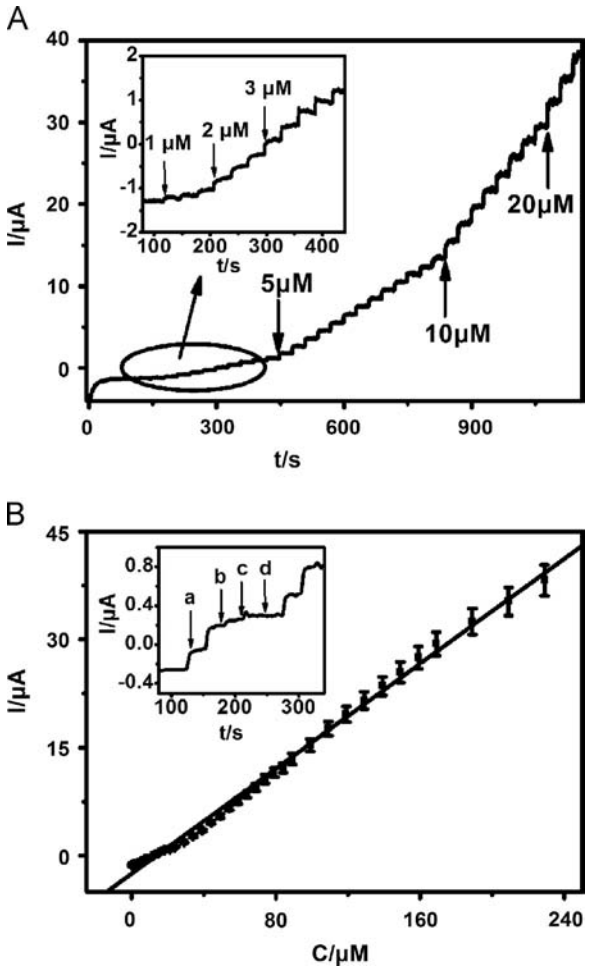

Fig. 8. (A) The amperometric *i*–*t* curve of OMCs-PDA/Pt with successive additions of N_2H_4 at the potential of −0.19 V. Inset shows the amplification of amperometric response of N_2H_4. (B) The corresponding calibration plot for N_2H_4 (RSD=5.6%, n=5). Inset shows the amperometric response of OMCs-PDA/Pt towards 2 μM N_2H_4 (a), 100 μM KNO_3 (b), $MgSO_4$ (c), and NH_4Cl (d).

detection of N_2H_4 at OMCs–PDA/Pt/Nafion/GC electrode. When the OMCs-PDA/Pt/Nafion/GC electrode was stored at 4 °C for two weeks, the amperometric response for 5 mM N_2H_4 remained 92.1% of its original value, suggesting the long-term stability of the electrode. The relative standard deviation of the amperometric response towards 5 mM N_2H_4 is less than 4.3% for five repetitive measurements at the same electrode, demonstrating the excellent reproducibility of the electrode.

4. Conclusions

In summary, a facile and effective approach is developed to prepare the OMCs-PDA/Pt nanocomposite. PDA-coated OMCs are easily prepared through one-step self-polymerization of DA on OMCs matrix at room temperature without any hard acid or radical initiator treatment. Pt NPs are deposited on OMCs-PDA *via* a simple microwave reduction method. After PDA modification, the dispersibility and water-solubility of OMCs are improved. The abundant amino and catechol groups of PDA are helpful for uniformly grafting charged metal complex $[PtCl_6]^{2-}$ that can be transformed into Pt NPs upon reduction, dispersing these Pt NPs and then generating ultra-fine Pt NPs with enhanced electrocatalytic ability. The obtained OMCs-PDA/Pt/Nafion/GC electrode exhibits significantly improved electrocatalytic responses towards H_2O_2 reduction and N_2H_4 oxidation compared with the OMCs/Pt/Nafion/GC and OMCs/Nafion/GC. In addition, this new nanocomposite modified electrode exhibits high sensitivity, good anti-interference ability, excellent reproducibility and long-term stability. The electrochemical properties and electrocatalytic ability of the modified electrode make OMCs-PDA/Pt nanocomposite promising for being developed as a new electrode material for electrochemical sensors and biosensors.

Acknowledgments

The authors gratefully acknowledge the financial support of the National Natural Science Foundation of China (21075014).

References

[1] R. Ryoo, S.H. Joo, S. Jun, J. Phys. Chem. B 103 (1999) 7743–7746.
[2] W.C. Choi, S.I. Woo, M.K. Jeon, J.M. Sohn, M.R. Kim, H.J. Jeon, Adv. Mater. 17 (2005) 446–451.
[3] Z. Wen, J. Liu, J. Li, Adv. Mater. 20 (2008) 743–747.
[4] L. Zou, M. Ren, H. Zhang, Z. Zou, H. Yang, S. Feng, Int. J. Electrochem. Sci. 8 (2013) 6180–6190.
[5] J. Tang, T. Wang, X. Sun, Y. Hu, Q. Xie, Y. Guo, H. Xue, J. He, Electrochim. Acta 90 (2013) 53–62.
[6] H.I. Lee, S.H. Joo, J.H. Kim, D.J. You, J.M. Kim, J.-N. Park, H. Chang, C. Pak, J. Mater. Chem. 19 (2009) 5934–5939.
[7] J.R.C. Salgado, J.J. Quintana, L. Calvillo, M.J. Lazaro, P.L. Cabot, I. Esparbe, E. Pastor, Phys. Chem. Chem. Phys. 10 (2008) 6796–6806.
[8] Y.S. Choi, S.H. Joo, S.-A. Lee, D.J. You, H. Kim, C. Pak, H. Chang, D. Seung, Macromolecules 39 (2006) 3275–3282.
[9] M.J. Lázaro, L. Calvillo, E.G. Bordejé, R. Moliner, R. Juan, C.R. Ruiz, Microporous Mesoporous Mater. 103 (2007) 158–165.
[10] H. Lee, S.M. Dellatore, W.M. Miller, P.B. Messersmith, Science 318 (2007) 426–430.
[11] W. Ye, H. Hu, H. Zhang, F. Zhou, W. Liu, Appl. Surf. Sci. 256 (2010) 6723–6728.
[12] Q.-L. Zhang, T.-Q. Xu, J. Wei, J.-R. Chen, A.-J. Wang, J.-J. Feng, Electrochim. Acta 112 (2013) 127–132.
[13] R. Baron, M. Zayats, I. Willner, Anal. Chem. 77 (2005) 1566–1571.
[14] Y. Fu, P. Li, Q. Xie, X. Xu, L. Lei, C. Chen, C. Zou, W. Deng, S. Yao, Adv. Funct. Mater. 19 (2009) 1784–1791.
[15] S.H. Joo, S.J. Choi, I. Oh, J. Kwak, Z. Liu, O. Terasaki, R. Ryoo, Nature 412 (2001) 169–172.
[16] Y. Sun, L. Zhuang, J. Lu, X. Hong, P. Liu, J. Am. Chem. Soc. 129 (2007) 15465–15467.
[17] A.A. Karyakin, E.E. Karyakina, L. Gorton, Anal. Chem. 72 (2000) 1720–1723.
[18] K. Yamada, K. Yasuda, N. Fujiwara, Z. Siroma, H. Tanaka, Y. Miyazaki, T. Kobayashi, Electrochem. Commun. 5 (2003) 892–896.
[19] J. Lu, C. Lau, M. Morizono, K. Ohta, M. Kai, Anal. Chem. 73 (2001) 5979–5983.
[20] M.C. Chang, A. Pralle, E.Y. Isacoff, C.J. Chang, J. Am. Chem. Soc. 126 (2004) 15392–15393.
[21] N. Higashi, H. Yokota, S. Hiraki, Y. Ozaki, Anal. Chem. 77 (2005) 2272–2277.
[22] X. Bian, X. Lu, E. Jin, L. Kong, W. Zhang, C. Wang, Talanta 81 (2010) 813–818.
[23] J.S. Budkuley, Microchim. Acta 108 (1992) 103–105.
[24] H. Seifart, W. Gent, D. Parkin, P. Van Jaarsveld, P. Donald, J. Chromatogr. B 674 (1995) 269–275.
[25] S. Plunkett, M.E. Parrish, K.H. Shafer, J.H. Shorter, D.D. Nelson, M.S. Zahniser, Spectrochim. Acta Part A 58 (2002) 2505–2517.
[26] S. Ameen, M. Shaheer Akhtar, H.S. Shin, Talanta 100 (2012) 377–383.
[27] D. Zhao, J. Feng, Q. Huo, N. Melosh, G.H. Fredrickson, B.F. Chmelka, G.D. Stucky, Science 279 (1998) 548–552.
[28] S. Jun, S.H. Joo, R. Ryoo, M. Kruk, M. Jaroniec, Z. Liu, T. Ohsuna, O. Terasaki, J. Am. Chem. Soc. 122 (2000) 10712–10713.
[29] W. Yu, W. Tu, H. Liu, Langmuir 15 (1999) 6–9.
[30] W. XiangáChen, J. YangáLee, Chem. Commun. 21 (2002) 2588–2589.
[31] J. Yang, T. Deivaraj, H.-P. Too, J.Y. Lee, Langmuir 20 (2004) 4241–4245.
[32] J. Ou, J. Wang, S. Liu, J. Zhou, S. Yang, J. Phys. Chem. C 113 (2009) 20429–20434.
[33] J. Jiang, L. Zhu, L. Zhu, B. Zhu, Y. Xu, Langmuir 27 (2011) 14180–14187.
[34] W. Zhang, J. Chen, G.F. Swiegers, Z.-F. Ma, G.G. Wallace, Nanoscale 2 (2010) 282–286.
[35] Y.-G. Zhou, J.-J. Chen, F.-b. Wang, Z.-H. Sheng, X.-H. Xia, Chem. Commun. 46 (2010) 5951–5953.
[36] X. Zhang, X. Shi, C. Wang, Catal. Commun. 10 (2009) 610–613.
[37] F. Jiang, R. Yue, Y. Du, J. Xu, P. Yang, Biosens. Bioelectron. 44 (2013) 127–131.
[38] L.-C. Chang, H.-N. Wu, C.-Y. Lin, Y.-H. Lai, C.-W. Hu, K.-C. Ho, Nanoscale Res. Lett. 7 (2012) 1–8.
[39] M. Liu, R. Liu, W. Chen, Biosens. Bioelectron. 45 (2013) 206–212.
[40] Y. Xia, W. Li, M. Wang, Z. Nie, C. Deng, S. Yao, Talanta 107 (2013) 55–60.
[41] A.-J. Wang, Q.-C. Liao, J.-J. Feng, Z.-Z. Yan, J.-R. Chen, Electrochim. Acta 61 (2012) 31–35.
[42] S. Ameen, M.S. Akhtar, H.S. Shin, Sens. Actuators, B 173 (2012) 177–183.
[43] Q. Yi, F. Niu, W. Yu, Thin Solid Films 519 (2011) 3155–3161.